BigBite Optics Summary

Diana Parno

September 13, 2010

Contents

1 Apparatus and Coordinate Systems **1**

2 First-Order Optics Model **2**
2.1 First-Order Momentum 3
2.2 First-Order Interaction Vertex 5

3 Calibration **5**
3.1 Correlation Variables 5
3.2 Apparatus Positions 6
3.3 Vertex Calibration 6
3.4 Angle Calibration 8
3.5 Momentum Calibration 9
3.6 Optics Quality Checks 10

4 Implementation in Analyzer Code **11**
4.1 Database File 11
4.2 Optics Class 12

In this document, I will summarize the algorithm and implementation of the optics package for BigBite, as developed by Xin Qian for the Transversity experiment (E06-010), and as inherited by the d2n experiment (E06-014).

1 Apparatus and Coordinate Systems

BigBite is a large-acceptance spectrometer that was situated to beam right during E06-010 (30° from the beamline) and E06-014 (45° from the beamline). Apart from the BigBite magnet itself, the spectrometer consists of a set of multi-wire drift chambers, a gas Cerenkov, and pre-shower and shower detectors. A sieve may optionally be mounted on the magnet face (between the magnet and the target) for calibration runs. Tracks are located in the recorded data by a pattern match tracking algorithm that looks for a valid hit pattern in the wire chambers, using templates of steadily increasing resolution. For added speed, this algorithm may be configured to include the BigBite calorimeter as a special "plane"; this functionality may be turned on or off via a flag in the database [1].

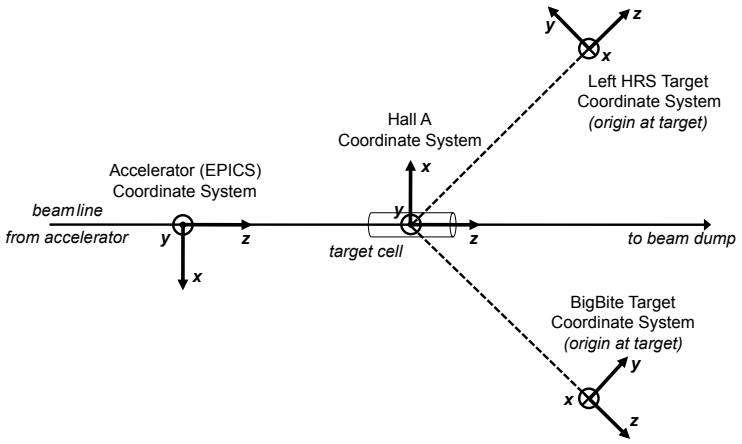

Figure 1: A schematic of four coordinate systems in common use in Hall A. Here, the beamline is seen from above, with the downstream direction toward the right of the figure.

There are several coordinate systems that are useful in describing tracks in a spectrometer; the relationship of four such coordinate systems to each other is shown in Figure 1. First are the two lab coordinate systems, which place the z axis along the beamline (with increasing z downstream) and the y axis vertically up. The two x axes differ, however. In the Accelerator coordinate system, used for EPICS beam position variables among other things, x is defined so as to make the coordinate system left-handed; the Hall A coordinate system, typically taken as "lab" coordinates by experimenters, is right-handed [2].

We can also define a target coordinate system for each spectrometer, so named because the origin is in the target (where the central ray of the spectrometer intersects with the z axis in the Hall A system). Here, the z axis points down the central ray of the spectrometer, away from the target and parallel to the floor. The x axis points downward (with gravity); note that the x_{tg} axis is vertical whereas the x_{Hall} axis is horizontal. The y axis, which is parallel to the floor, is defined so as to form a right-handed coordinate system: $\hat{y} = \hat{z} \times \hat{x}$.

Finally, each spectrometer has a set of detector coordinates (not shown in the figure), which simplify the description of tracks. For BigBite, the detector coordinate system has its origin in the center of the first multi-wire drift chamber plane. The z axis is the nominal direction of the particle passing through the chamber; the x axis points downward with gravity; and the y axis is once again defined to form a right-handed coordinate system. [3].

2 First-Order Optics Model

The goal of an optics package is to take a track through the chambers and relate it to the trajectory of the detected particle immediately after it scattered from the nuclear target. This is made challenging by the fact that our charged particle has passed through an imperfectly understood magnetic field between the target and our detectors. A careful modeling and calibration of the optics allows us to derive both a position for the initial vertex (i.e. scattering interaction) and also the momentum of the particle just after scattering, based on the position and direction of its observed track in the spectrometer.

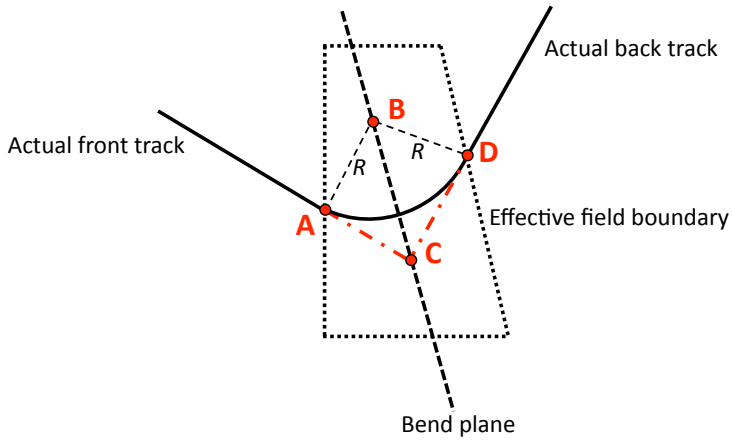

Figure 2: A schematic of the E06-010 implementation of the effective bending plane model for BigBite. Angles are exaggerated for clarity.

In defining a first-order model of the BigBite optics, we take as a starting point the assumption that the BigBite magnet is a perfect dipole – i.e. that its magnetic field is uniform throughout its volume. The particle trajectory in the magnetic field therefore describes an arc of a circle with radius R. Outside the volume of the magnet (defined by some effective field boundary), we assume that the magetic field is zero. Deviations from this model can be corrected in later iterations of the optics calibration process.

Our next assumption is that we can model the particle's interactions with the BigBite magnetic field using an effective bending plane. In this model, we reduce all interactions between the particle and the magnet to a single "bend" at the effective bending plane, which bisects the magnet. In the *front track*, before it reaches the bending plane, the particle is assumed to travel in a straight line, even when it is technically within BigBite's magnetic field; in the *back track*, after it has crossed the bending plane, the particle travels a straight line deflected by some angle from its original path. This latter track is what is picked up in the wire chambers. [4]

Figure 2 defines the geometry of the first-order optics model as implemented for E06-010. The solid line shows the actual trajectory of the charged particle; the dotted line shows the effective field boundary of the magnet. The particle enters the magnetic field at point A and leaves it at point D. We model its interactions as occurring at a single point C on the bend plane (thick dashed line); its path through the magnetic field is then given by two straight-line segments $\overline{AC}$ and $\overline{CD}$ (red dash-dotted lines). The center of the bending arc, part of a circle with radius R, is at point B. We define $L = \overline{AC} + \overline{CD}$ as the distance traveled in the magnetic field in this model, noting that $\overline{AC} = \overline{CD} = L/2$ since the bend plane bisects the bending arc.

2.1 First-Order Momentum

Because $\overline{AC}$ is tangent to the arc of curvature, it is perpendicular to the radius $\overline{AB}$, making angle $\angle BAC$ a right angle. If we define $\theta_{bend} = \angle ABD$ as the angle through which the particle trajectory bends in the plane perpendicular to the magnetic field, then $\theta_{bend}/2 = \angle ABC$ and we can express the radius of curvature R as

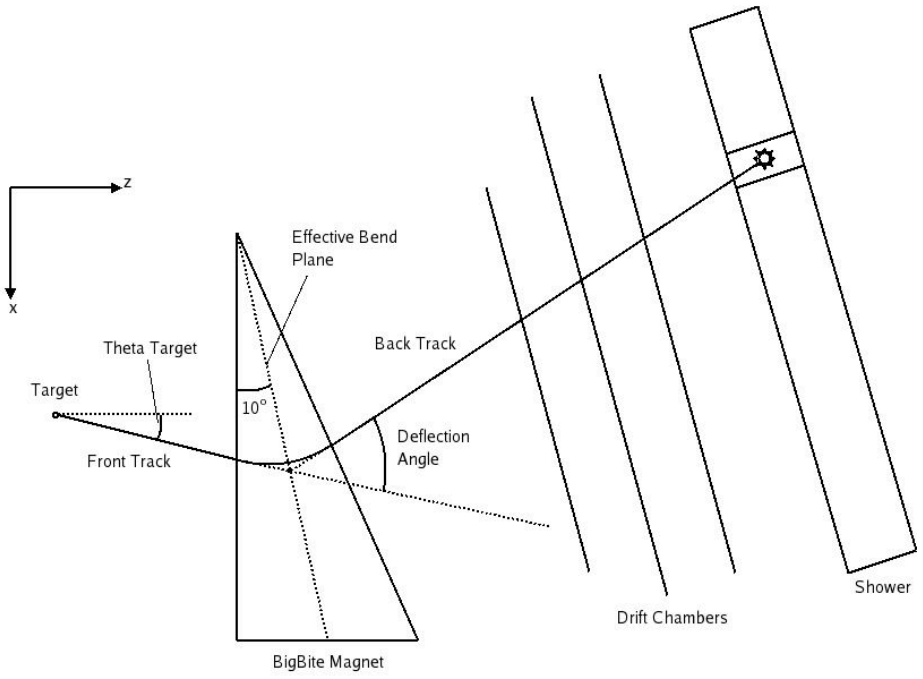

Figure 3: A side-view, not-to-scale diagram of the effective bending plane model for BigBite, reproduced from [4].

$$R = \frac{L}{2\tan\left(\frac{\theta_{bend}}{2}\right)} \tag{1}$$

We note that, in Figure 2, the deflection angle used in several other optics packages (defined in, for example, Figure 3) is the supplementary angle to $\angle ACD$.

From the radius of curvature, we can derive the momentum component $p_\perp$ perpendicular to the magnetic field direction. For a magnetic field of magnitude B, this is

$$p_\perp = |q|BR = \frac{|q|LB}{2\tan\left(\frac{\theta_{bend}}{2}\right)} \tag{2}$$

In order to compute the total momentum of the particle, rather than just that component perpendicular to $\mathbf{B}$, we require one more angle, not shown in Figure 2, to complete our picture. We define ϕ as the angle between the particle momentum and the magnetic field; in the approximation of BigBite as a perfect dipole, ϕ for any given track is fixed throughout the volume of the magnet.

$$\cos\phi = \frac{\mathbf{B}\cdot\mathbf{p}}{|B||p|} \tag{3}$$

The perpendicular momentum component $p_\perp$ is related to the magnitude p of the total momentum by $p_\perp = p\sin\phi$. Equation 2 thus leads us to a first-order expression for the magnitude of the complete electron momentum:

$$p = \frac{LB}{2 \sin\phi \tan\left(\frac{\theta_{bend}}{2}\right)} \tag{4}$$

Here, we have set the electron charge q to -1.

2.2 First-Order Interaction Vertex

Determining the momentum according to this method requires on a good first-order determination of $\overline{AC}$ and thus of the front track and the vertex of the scattering interaction. This problem, too, is simplified by the effective bending plane model. First, the back track reconstructed in the multi-wire drift chambers is extrapolated back to find the point C where it intersects with the bend plane. We assume that the front track must also intersect the bend plane at the same point. Furthermore, any valid front track must make the same angle ϕ with the magnetic field that the back track does. At this stage, the complete set of possible solutions to the front-track problem forms a cone with an apex at C and an opening angle of ϕ.

This cone of solutions will intersect with the beamline; since ϕ is fairly large, there will be only one intersection point within a reasonable distance of the nominal target. This intersection point defines the first-order interaction vertex, and the front track becomes the line connecting this vertex to the bend plane at C. [1]

3 Calibration

The first-order optics model is only a beginning: BigBite is not a perfect dipole, necessitating corrections both to the interaction vertex and to the momentum. In E06-010, these corrections were determined using data from both first-pass (1.2306 GeV) and second-pass (2.396 GeV), in a six-step process [1]. In E06-014, where BigBite was positioned at a different angle, there is enough optics data to redo the lower-order calibrations, but the higher-order calibration constants must be taken directly from the E060-010 results.

3.1 Correlation Variables

In a non-uniform magnet, the trajectory of a charged particle will depend on the particular regions of the magnetic field that it traverses. This manifests itself in the data as correlations between discrepancies and variables describing the location and direction of the particle trajectory. We use a set of six variables to describe how and where the particle passes through the magnetic field.

The first pair, x and y, define the hit position (in detector coordinates) of the reconstructed track in the first wire chamber. The second pair, x' and y' (also known as, respectively, θ_{targ} and ϕ_{targ} [4]), define the track's direction in the detector coordinate system:

$$x' = \frac{dx_{det}}{dz_{det}} \tag{5}$$

$$y' = \frac{dy_{det}}{dz_{det}} \tag{6}$$

The final pair of relevant variables are x_{bend} and y_{bend}, which specify the position (in detector coordinates) of point C, the location where the track intersects the effective bending plane.

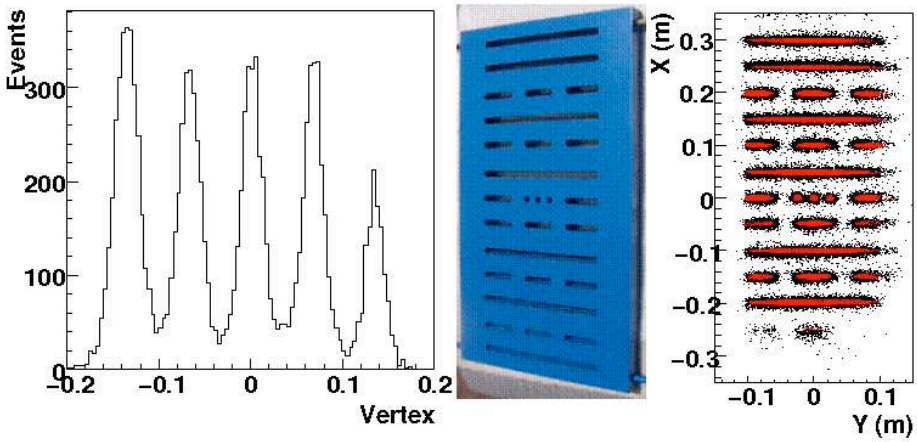

Figure 4: Results from the no-field calibration of the BigBite optics for E06-010, reproduced from [1]. At left is the reconstructed interaction vertex, showing the individual foils of the target. In the center is a photograph of the BigBite sieve. At right is the sieve pattern reconstructed from the data; black points indicate the intersections of tracks with the sieve plane, while red points highlight those tracks that, geometrically, should have passed through a sieve slit.

3.2 Apparatus Positions

The first step involved obtaining the positions of the target and of the BigBite magnet (via the sieve position) from Hall A survey reports; without knowing these relative positions, it would be impossible to reconstruct the front track. The survey reports also gave initial values for the wire chamber positions, which allowed a more accurate first-order optics model.

In the second step, the positions of the wire chamber were improved and finalized empirically, using runs where the BigBite magnet was turned off. Without any bending by the magnetic field, the front track would align perfectly with the back track, and a good reconstruction of the sieve pattern would indicate accurate positions for the wire chamber. Figure 4 shows the E06-010 results from this stage of the calibration.

3.3 Vertex Calibration

The third step was to improve the reconstruction of the interaction vertex. In runs with a multifoil carbon target and the sieve removed from the BigBite magnet face, the first-order vertex-z position $Z_v^{(0)}$ (in Hall A coordinates) could be compared to the absolute reference of that foil's surveyed position. The discrepancy in Z_v may be correlated to one of the six variables defined in Section 3.1. Studying these correlations allows us to define first- and second-order corrections for the vertex-z position:

$$Z_v^{(1)} = Z_v^{(0)} + b_1 + a_1 y \tag{7}$$

$$
\begin{aligned}
Z_v^{(2)} = Z_v^{(1)} &+ \left(a_{20} + a_{21} Z_v^{(1)}\right) + x\left(b_{20} + b_{21} Z_v^{(1)}\right) \\
&+ \left(a_{22} + a_{23} Z_v^{(1)}\right) + y\left(b_{22} + b_{23} Z_v^{(1)}\right) \\
&+ \left(a_{24} + a_{25} Z_v^{(1)}\right) + x'\left(b_{24} + b_{25} Z_v^{(1)}\right) \\
&+ \left(a_{26} + a_{27} Z_v^{(1)}\right) + y'\left(b_{26} + b_{27} Z_v^{(1)}\right) \\
&+ \left(a_{28} + a_{29} Z_v^{(1)}\right) + x_{bend}\left(b_{28} + b_{29} Z_v^{(1)}\right) \\
&+ \left(a_{30} + a_{31} Z_v^{(1)}\right) + y_{bend}\left(b_{30} + b_{31} Z_v^{(1)}\right)
\end{aligned}
\tag{8}
$$

There is some redundancy in the expression of Equation 8: to show more clearly that the coefficients of each line of the equation are determined independently (in a separate calibration for each variable), the a_{mn} terms have not been recombined, nor have coefficients which go to zero been removed.

Optics corrections are an iterative process, and the procedure defined by Equation 8 was immediately repeated to give the third-order vertex position Z_v^3. At this stage, the discrepancies were resolved as well as they could be using only the six variables describing the track position and direction; the next phase of the vertex calibration required the inclusion of momentum-dependent corrections. Using the front track defined by Z_v^3, a first-order momentum $p^{(0)}$ was computed from Equation 4. Then first- and second-order corrections – only approximate, due to the wide momentum spectrum of scattering from a carbon-foil target – were defined, based on momentum variations with the six track direction and position variables:

$$
\begin{aligned}
p^{(1)} = p^{(0)} &\cdot \left(c_0 + c_1 y_{bend} + c_2 y_{bend}^2\right) \\
&\cdot \left(d_0 + d_1 x_{bend}\right) \\
&\cdot \left(e_0 + e_1 Z_v^{(3)}\right) \\
&\cdot \left(f_0 + f_1 x + f_2 x^2\right) \\
&\cdot \left(g_0 + g_1 x' + g_2 x'^2\right) \\
&\cdot \left(h_0 + h_1 y + h_2 y^2\right) \\
&\cdot \left(i_0 + i_1 y' + i_2 y'^2\right)
\end{aligned}
\tag{9}
$$

$$
\begin{aligned}
p^{(2)} = p^{(1)} &\cdot \left(j_0 + j_1 x_{bend} + j_2 x_{bend}^2\right) \\
&\cdot \left(k_0 + k_1 y_{bend} + k_2 y_{bend}^2\right) \\
&\cdot \left(l_0 + l_1 p^{(1)}\right)
\end{aligned}
\tag{10}
$$

By examining the correlation of the vertex discrepancy with the approximate second-order momentum $p^{(2)}$, we can obtain coefficients for momentum-dependent vertex corrections:

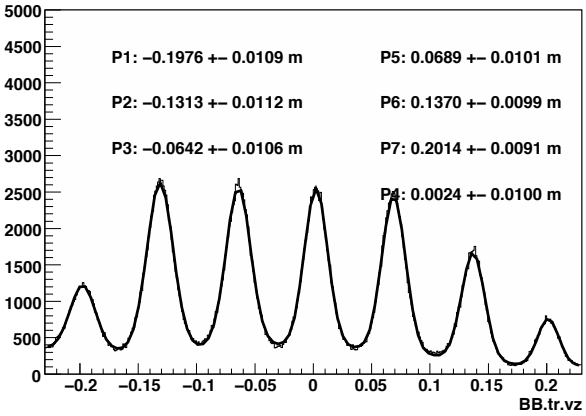

Figure 5: Final results of the E06-010 vertex position calibration, done for a representative momentum value of 0.9 GeV/c and reproduced from [1].

$$Z_v^{(4)} = Z_v^{(3)} - x_{bend} Z_v^{(3)} \left(m_0 + m_1 p^{(2)} \right) + \left(n_0 + n_1 Z_v^{(3)} \right) \left(o_0 + o_1 p^{(2)} \right) + e^{\left(p_0 + p_1 p^{(2)} \right) \left(q_0 + q_1 Z_v^{(3)} \right)} \tag{11}$$

A second round of momentum-dependent corrections, done according to Equation 11, resulted in a fifth-order vertex position $Z_v^{(5)}$.

The final set of vertex corrections relied on a set of lookup tables. The three-dimensional phase space described by $(x_{bend}, y_{bend}, Z_v)$ can be delineated by a fine grid. Any point within the phase space is contained within a cubical volume defined by eight corners with various values of x_{bend}, y_{bend}, and $Z_v^{(m)}$; a linear interpolation between those corners gives the nth-order vertex position $Z_v^{(n)}$. Two additional lookup tables are defined for the phase spaces $\left(x_{bend}, p^{(2)}, Z_v\right)$ and $\left(y_{bend}, p^{(2)}, Z_v\right)$. The final three orders of vertex positions are thus defined by

$$Z_v^{(6)} = f_1 \left(x_{bend}, y_{bend}, Z_v^{(5)} \right) \tag{12}$$

$$Z_v^{(7)} = f_2 \left(x_{bend}, p^{(2)}, Z_v^{(6)} \right) \tag{13}$$

$$Z_v^{(8)} = f_3 \left(y_{bend}, p^{(2)}, Z_v^{(7)} \right) \tag{14}$$

where f_1, f_2 and f_3 are the linear interpolation functions. Figure 5 shows the final results for a momentum value of 0.9 GeV/c.

3.4 Angle Calibration

The fourth step of the optics calibration relied on runs with both carbon and hydrogen gas targets, taken with the sieve positioned in front of the magnet. The goal was to improve on the first-order

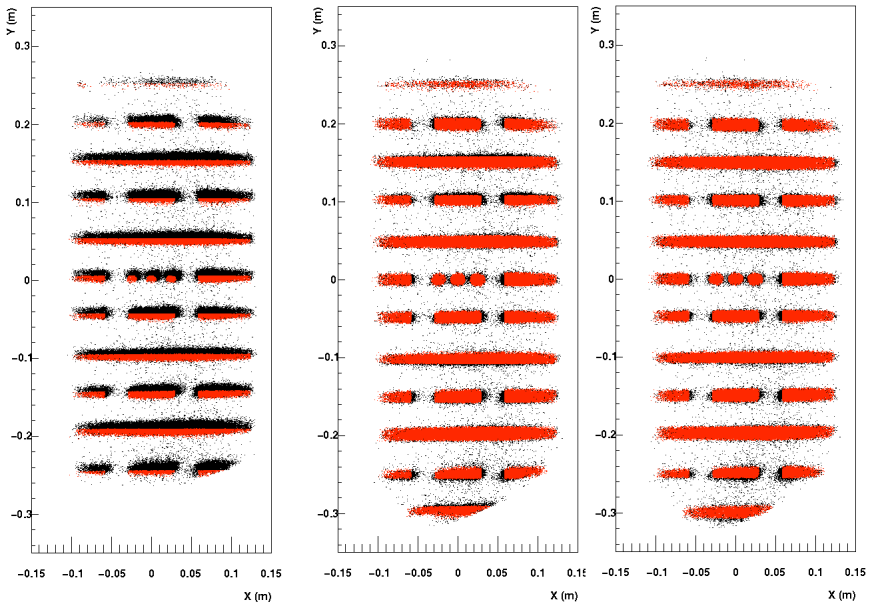

Figure 6: Procedure for calibrating the angles used in the optics model, reproduced from [1]. Black points indicate the intersections of tracks with the sieve plane, while red points highlight those tracks that, according to the geometrical model, should have passed through a sieve slit. The left panel shows results using the first-order model of the angles. In the middle, we see the improvement that is made by applying a constant offset. At right is the final sieve pattern, incorporating high-order corrections to the angles.

estimates of angles ϕ and θ_{bend} (defined in Section 2.1), which are determined from the front track connecting the final vertex position and the middle point C on the bend plane. Figure 6 outlines the procedure for this calibration. The first-order model (left) results in an expected sieve pattern (red) that is systematically lower than the actual one (black). Offsets result in better agreement (middle), and performing an analogous procedure to that for vertex reconstruction (Section 3.3) gives the best agreement of all (right).

3.5 Momentum Calibration

With trustworthy values for the vertex position and angles in hand, elastic scattering data from H_2 target runs could be used to perform an exact calibration of the momentum. The final momentum $p_{elastic}$ of an elastically scattered electron can be calculated exactly from its initial momentum p_i and its scattering angle θ:

$$p_{elastic} = \frac{p_i M}{M + p_i\,(1 - \cos\theta)} \tag{15}$$

where M is the mass of the other particle in the elastic scattering interaction. (The electron mass is assumed to be negligible compared to M). The reconstructed momentum of an electron that undergone elastic scattering from a proton should match the expected momentum $p_{elastic}$ for its observed scattering angle θ; if it does not, the momentum reconstruction requires correction.

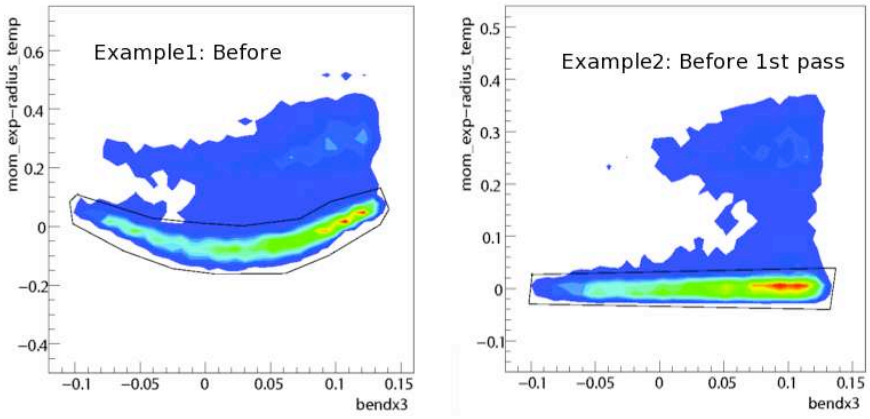

Figure 7: Sample graphical cuts on plots of δp (before calibration) versus x_{bend}, reproduced from [1]. At left is a region at the bottom of the magnet; at right is a region near the center of the magnet. Events within the black outline are taken to be elastic events.

The first stage of the momentum calibration must be to identify events corresponding to elastic scattering from a proton. To a large extent, this may be achieved via particle identification (for example, cuts on the Cerenkov signal to remove most particles that are not electrons) and by trigger information. If elastic-scattering calibration runs are taken with BigBite and the Left HRS in coincidence, and if the Left HRS is configured to detect protons at an appropriate angle, then a coincidence trigger is evidence that both a proton and an electron were involved in the scattering interaction.

For the E06-010 calibration, event selection was done partly by means of the discrepancy δp between the reconstructed momentum and $p_{elastic}$. Where elastic scattering events dominate the sample, values of δp in a given region of the magnet will form a relatively narrow peak, even if the peak is offset from zero. Events in this peak may be selected as elastically scattered electrons and used for calibration of the reconstructed momentum. In the end, this was accomplished by dividing events into small regions according to the value of y_{bend}. Within each region, δp was plotted against x_{bend}, and a graphical cut was used to select the high-intensity region corresponding to elastic electrons. Figure 7 shows examples of graphical cuts in two regions of the magnet.

In contrast to the calibration procedure for the vertex position, all momentum corrections to the first-order model of Equation 4 were done with a lookup table. The position of each track in the two-dimensional phase space defined by (x_{bend}, y_{bend}) was used to find the linear interpolation of the relevant correction, based on the values of the correction function at neighboring points in the phase space grid. Where the $z_n\,(x_{bend}, y_{bend})$ are linear interpolation functions, the final momentum correction can be expressed as

$$p^{(1)} = z_0\,(x_{bend}, y_{bend})\,p^{(0)} + z_1\,(x_{bend}, y_{bend}) + z_2\,(x_{bend}, y_{bend})\,x + \frac{z_3\,(x_{bend}, y_{bend})}{\theta_{bend}} \qquad (16)$$

3.6 Optics Quality Checks

When the BigBite optics are calibrated at low beam energies (1.23 GeV and 2.4 GeV) and production data are taken at higher beam energies, it is desirable to confirm that the calibrations are

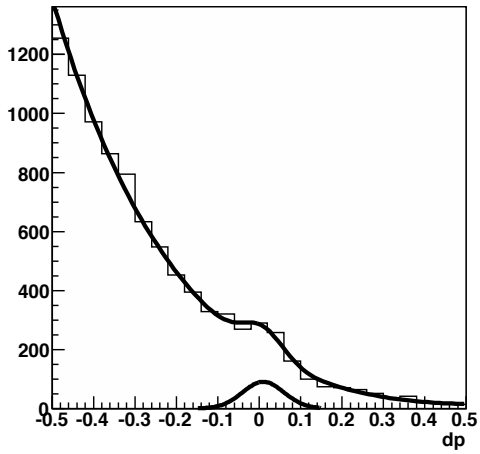

Figure 8: Momentum discrepancy δp for a hydrogen-target run with five-pass beam, reproduced from [1].

still valid at higher energies. For example, does analysis of a multifoil-target run at 5.9 GeV still produce vertex positions that coincide with the known position of the foils?

At low beam energies, the peak locations in W for known nuclear resonances (e.g. the $\Delta(1232)$ for one-pass beam or the $\Delta(1232)$, N(1520), N(1700) and $\Delta(1700)$ for two-pass beam) can provide important evidence that the momentum calibration is valid beyond the special case of elastic scattering from the proton. At higher beam energies, elastic scattering events no longer dominate the sample, but it may still be possible to pick out such events in data with a hydrogen target. Figure 8 shows the distribution of δp, the discrepancy between the reconstructed momentum and the momentum expected for elastic scattering, for a run at 5.9 GeV during E06-010. The small peak at $\delta p = 0$ shows events due to elastic scattering; that this peak is well-aligned at 0 is evidence that the reconstructed momentum is still valid at this high energy.

During E06-014, we have access to some hydrogen data at beam energies of 5.9 GeV; a target operator error on February 18, 2009, led to two and a quarter hours of running with H_2 (rather than N_2) in the reference cell [5].

4 Implementation in Analyzer Code

The class `THaOpticsE06010` was written to form part of the Big Bite analysis library (`bigbitelib`) for the Transversity data analysis. In a replay script, the `THaBigBite::MountOptics` command allows the user to specify this optics module, which is then used to analyze each track. Mounting an optics module requires the specification of a beam module; this is typically set to be the unrastered beam.

4.1 Database File

The database file `db_BB.optics.dat` stores optics parameters for a variety of optics classes, including the default `THaOptics`, the G_E^n optics class `THaOpticsAGen`, and even `THaOpticsHRS`. It is unknown when these parameters were last updated.

The section of the database file for the Transversity optics package includes two flags which toggle various parts of the analysis: `nofield_flag`, when enabled, turns off all calibrations having to do with the magnetic field, and `calib_flag`, when enabled, turns on the software which determines whether a given track ought to have passed through a slot in the sieve. In the database file applying to all E06-014 run periods, `nofield_flag` is presently disabled and `calib_flag` is enabled.

Eighteen double-precision parameters encode the position and Euler angles of the effective bending plane, the sieve plate (and thus the magnet), and the first wire chamber. These positions and angles were determined from calibrations performed by Xin Qian.

The remaining two-thousand-odd lines of the database file encode the various lookup tables for vertex and momentum reconstruction in both negative and positive optics. Lower-order corrections, such as the a_{mn} and b_{mn} coefficients in Equation 8 for $Z_v^{(2)}$, are hard-coded into the optics class itself.

4.2 Optics Class

The `THaOpticsE06010` class was not designed to be directly applicable to other experiments. Many important parameters – from the locations of the target foils to the exact slot pattern in the sieve plate – are typed directly into the compiled code. Therefore, great care must be taken when making modifications or considering changed configurations. For example, the code was developed for a single current setting of the BigBite magnet, and is unlikely to work for other settings.

The primary method of the class is `ApplyOptics`, of which there are three overloaded versions; nearly all the work is done by the third, which takes six explicit input arguments (various parameters of the track and of the beam) and seven explicit output arguments (momentum, vertex, path length, and position and angle variables in the target coordinate system). Over the course of this function, numerous observables are computed:

- The *particle charge* is determined through cuts on the relationship between the x and x' variables. (The existence of a magnetic field is not required for this determination; of course, the charge cannot be trusted if the magnetic field is off.)

- The *vertex position* is calculated according to the procedure outlined in Section 3.3. The calibration constants are different for positive and negative optics. Some additional corrections are made to the preliminary momentum used in this calibration, but only if this preliminary value is below 3 GeV/c. Much of the vertex calculation is done in a coordinate system defined by the sieve plane.

- The *momentum* is calculated according to the procedure outlined in Section 3.3. Additional corrections are made for the low-momentum case of $p < 0.9$ GeV/c, shifting the momentum result to a lower value (the shift is proportional to the momentum itself). The variable used to keep track of the momentum is labeled `radius`.

- The *energy loss* for the outgoing electron is calculated based on the angle between the track direction and the beam direction. The radiation lengths presented by obstacles in the path of the outgoing electron are hard-coded. The final adjustment to the momentum due to energy loss is corrected both for the difference between the mean and most likely values in a Landau distribution, and for the fact that the initial momentum calibration was performed without regard for this difference in the energy loss for the incoming electron.

These, as well as some intermediate observables (such as x_{bend} and y_{bend}), are stored as private data members (and also as data members of a parallel `theoptics` class) and are accessible in the primary tree as part of the `BB.optics` variable block.

References

[1] X. Qian, *Measurement of single target-spin asymmetry in semi-inclusive $n^{\uparrow}(e, e'\pi^{\pm})$ reaction on a transversely polarized ^{3}He target*. Ph.D. thesis, Duke University (2010)

[2] C. Hyde-Wright, L. Todor, and G. Laveissiere, *Beam position studies for e93050*. Technical Report TN-01-001, JLAB (2001)

[3] K. Allada, *Measurement of single spin asymmetries in semi-inclusive deep inelastic scattering reaction $n^{\uparrow}(e, e'\pi^{+})X$ at Jefferson Lab*. Ph.D. thesis, University of Kentucky (2010)

[4] S. Riordan, *Measurements of the electric form factor of the neutron at Q^2 = 1.7 and 3.5 GeV^2*. Ph.D. thesis, Carnegie Mellon University (2008)

[5] V. Sulkosky, *Hall A Logbook entry: Runs 20248-20254 and 1564-1575 H2 not N2* (2009), URL `http://www.jlab.org/~adaq/halog/html/0902_archive/090218205206.html`